Sigma J Eng Nat Sci, Vol. 42, No. 6, pp. 1856−1865, December, 2024

Sigma Journal of Engineering and Natural Sciences
Web page info: https://sigma.yildiz.edu.tr
DOI: 10.14744/sigma.2024.00142

Research Article

Scrutiny of flow and heat transfer characteristics of hybrid nanofluid passing through a squeezing channel

Rohit SHARMA[1], Darapaneni ARUNA[1], Manoj Kumar MISHRA[2,*], Sneh Bala SINHA[1]

[1]*Department of Mathematics, School of Science, GITAM Deemed to be University - Bengaluru, Karnataka, 561203, India*
[2]*Department of Mathematics, School of Advanced Sciences, VIT - AP University, Andhra Pradesh, 522237, India*

ARTICLE INFO

Article history
Received: 26 August 2023
Revised: 13 October 2023
Accepted: 29 December 2023

Keywords:
Graphene; Heat Absorption; MHD; Nanofluid

ABSTRACT

This article mainly presents a comparative analysis of MHD flow of three different types of fluids, namely, simple base fluid (Ethylene Glycol), mono-nanofluid (Ethylene Glycol+Graphene) and Hybrid nanofluid (Ethylene Glycol+Graphene+Copper) passing through a squeezing channel. The effect of heat absorption and Joule dissipation is also taken into account. System of partial differential equation governing the flow problem is transformed into a system of ordinary differential equation by using similarity transforms. To get the solution, shooting technique along with Runge-Kutta 4th order method is employed. The influence of several physical parameter on velocity, temperature, skin friction and Nusselt number is analyzed. The findings indicate that temperature increases with the enhancement of a magnetic field and Joule dissipation. Moreover, the study reveals that the temperature of mono-nanofluid is higher than that of the base fluid but lower than that of the hybrid nanofluid.

Cite this article as: Sharma R, Aruna D, Mishra MK, Sinha SB. Scrutiny of flow and heat transfer characteristics of hybrid nanofluid passing through a squeezing channel. Sigma J Eng Nat Sci 2024;42(6):1856−1865.

INTRODUCTION

The increasing utilization of nanofluids in real-world industrial applications has made them a major focus of research. In 1995, Choi and Eastman [1] discovered that the addition of metallic nanoparticles enhances heat transfer. Buongiorno [2] identified seven methods to improve the heat transfer rate of base fluids, with Brownian motion and thermophoresis playing significant roles. Nanofluids find important applications in energy conversion, microsystems cooling, and the medical industry. Numerous researchers have investigated the heat transfer characteristics of nanofluids [3-7].

Graphene, with its notable properties such as thermal conductivity, flexibility, and high elasticity [8], has found various applications in batteries, supercapacitors, and miniaturized solar devices [9]. Upadhya et al. [10] conducted a study on enhancing the heat transfer rate using ethylene glycol with graphene nanoparticles. Bhattacharyya et al. [11] carried out the statistical analysis of the Ethylene glycol and graphene based nanofluid flow over a stretching sheet.

***Corresponding author.**
*E-mail address: manojmishra.iitg@gmail.com

This paper was recommended for publication in revised form by Editor-in-Chief Ahmet Selim Dalkilic

Published by Yıldız Technical University Press, İstanbul, Turkey

In recent years, researchers have focused on the use of hybrid nanofluids, which involve mixing multiple nanoparticles in a fluid, to further improve heat transfer rates. Devi and Devi [12] investigated the flow of a hybrid nanofluid (Cu-Al_2O_3/water) over a stretching sheet, presenting a novel mathematical model. Suresh et al. [13] validated this new model using experimental data. Devi and Devi [14] extended their work to study 3-dimensional flow under Newtonian heating conditions, finding higher heat transfer rates in hybrid nanofluids compared to regular nanofluids. Prakash and Devi [15] examined the influence of Al_2O_3–Cu/water nanofluid passing through a slender stretching sheet. Bahiraei and Mazaheri [16] explored the application of graphene-platinum hybrid nanofluids in miniature devices. Aziz et al. [17] investigated entropy generation due to hybrid nanofluids with Maxwell as the base fluid, considering radiation, magnetic fields, and joule heating. Yashkun et al. [18] studied hybrid nanofluid flow past an exponentially stretching/shrinking sheet, taking mixed convection into consideration. Rafique et al. [19] shows that heat transfer performance in hybrid nanofluid is better than mono-nanofluid.

Joule dissipation, a significant heat source in fluid flow under the influence of a magnetic field, plays a vital role in heat-treated materials. Rashid et al. [20] studied the impact of Joule heating on MHD flow over a stretchable wall of graphene–carboxymethyl cellulose (CMC) with water as a base fluid. Hence, several studies have examined the effect of Joule dissipation [21-23].

Flow within the channel is often observed in many engineering and industrial processes, for example, lubrication systems, moving pistons, hydraulic lifts, injection moulding, flow inside the nasogastric tubes syringes. Due to its nobility, many researchers analyzed the flow within the channel under various conditions [24, 25]. The flow induced by the compression of two parallel plates due to external applied stress is known as squeezing flow. The squeezing flow situation is often observed in many engineering and industrial processes. Noor and Shafie [26] discovered nature of hydromagnetic flow of hybrid nanofluid within squeeze channel. Due to its immense applications, the flow through a squeezing channel has attracted many researchers [27-30].

A careful review of the literature suggests that, no investigation has been conducted on comparative analysis for flow and heat transfer characteristics among three different fluids namely base fluid (Ethelene Glycol), mono-nanofluid (Ethelene Glycol + Graphene), and hybrid nanofluid (Ethelene Glycol + Graphene + Copper) passing through a squeezing channel taking into account of heat absorption and magnetic field effects. Thus, the present study analyses the impact of various physical parameters on base fluid, mono-nanofluid and hybrid nanofluid taking into account of these effects.

Modeling of the Problem

Consider 2-dimensinal electrically conducting, heat absorbing, radiating, incompressible, electrically conducting hybrid nanofluid flow within squeezing channel taking Joule dissipation into account. Our mathematical model is related to 2 parallel plates which is along x and z-axis and y is normal to the plates. The gap between two plates is $h(t) = H(1 - \alpha t)^{\frac{1}{2}}$ at time t. Direction and speed of plates is controlled by α. The velocity of plates is $\frac{dh}{dt}$ and the gap will be 0 between two plates at $t = \frac{1}{\alpha}$ $(\alpha \neq 0)$. Negative value of α denotes that distance between plates are increasing. Magnetic field is applied perpendicular to the surface of plates and strength is given by $B(t) = B_o(1 - \alpha t)^{-\frac{1}{2}}$. It is also assumed that there is no chemical reaction. Geometry of the problem express in Figure 1. Under these conditions, the mathematical model governing the boundary layer flow are given by [27]:

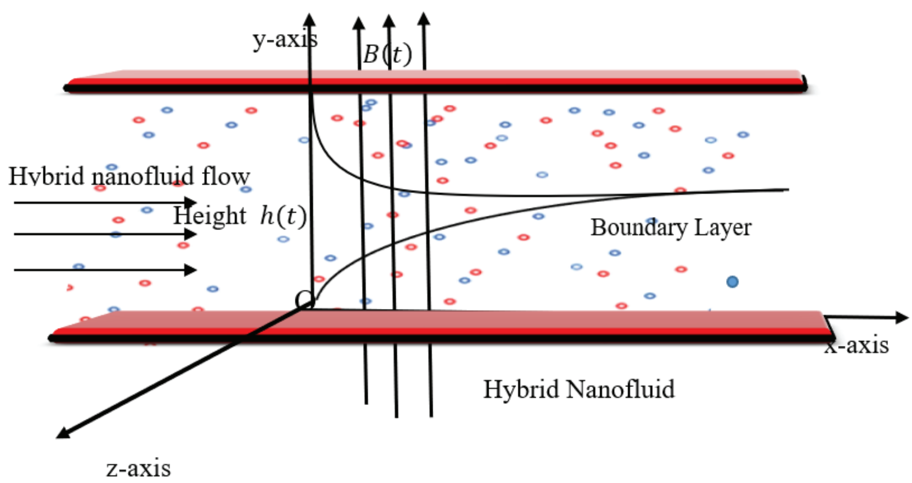

Figure 1. Geometry of the flow problem.

$$\frac{\partial u}{\partial x}+\frac{\partial v}{\partial y}=0, \tag{1}$$

$$\frac{\partial u}{\partial t}+u\frac{\partial u}{\partial x}+v\frac{\partial u}{\partial y}=-\frac{1}{\rho_{hnf}}\frac{\partial p}{\partial x}-\frac{\sigma_{hnf}B^2(t)\,u}{\rho_{hnf}}+\vartheta_{hnf}\left[\frac{\partial^2 u}{\partial x^2}+\frac{\partial^2 u}{\partial y^2}\right], \tag{2}$$

$$\frac{\partial v}{\partial t}+u\frac{\partial v}{\partial x}+v\frac{\partial v}{\partial y}=-\frac{1}{\rho_{hnf}}\frac{\partial p}{\partial y}+\vartheta_{hnf}\left[\frac{\partial^2 v}{\partial x^2}+\frac{\partial^2 v}{\partial y^2}\right], \tag{3}$$

$$\frac{\partial T}{\partial t}+u\frac{\partial T}{\partial x}+v\frac{\partial T}{\partial y}=\frac{K_{hnf}}{(\rho c_P)_{hnf}}\left[\frac{\partial^2 T}{\partial x^2}+\frac{\partial^2 T}{\partial y^2}\right]+\frac{\sigma_{hnf}B^2(t)u^2}{(\rho c_P)_{hnf}}-\frac{QT}{(\rho c_P)_{hnf}}. \tag{4}$$

Where, u and v are the velocity of hybrid nanofluid in x and y- directions. T indicates the temperature of fluid, p, ρ_{hnf}, μ_{hnf}, ϑ_{hnf}, $(\rho_{C_p})_{hnf}$, K_{hnf}, Q and σ_{hnf} denote the fluid pressure, density of hybrid nanofluid, kinematic viscosity of hybrid nanofluid, heat capacity of hybrid nanofluid, thermal conductivity of hybrid nanofluid, heat absorption coefficient and electrical conductivity of the hybrid nanofluid respectively. Properties of hybrid nanofluid are noted as [25]:

$$\rho_{hnf}=(1-\phi_2)[(1-\phi_1)\rho_f+\phi_1\rho_{n_2}]+\phi_2\rho_{n_1}, \tag{5}$$

$$(\rho c_p)_{hnf}=(1-\phi_2)\left[(1-\phi_1)(\rho c_p)_f+\phi_1(\rho c_p)_{n_1}\right]+\phi_2(\rho c_p)_{n_2}, \tag{6}$$

$$\mu_{hnf}=\frac{\mu_f}{(1-\phi_1)^{2.5}(1-\phi_2)^{2.5}}, \tag{7}$$

$$\frac{K_{hnf}}{K_f}=\left[\frac{K_{n_2}+2K_{nf}-2\phi_2(K_{nf}-K_{n_2})}{K_{n_2}+2K_{nf}+\phi_2(K_{nf}-K_{n_2})}\right], \tag{8}$$

$$\frac{\sigma_{hnf}}{\sigma_f}=\left[\frac{\sigma_{n_2}+2\sigma_{nf}-2\phi_2(\sigma_{nf}-\sigma_{n_2})}{\sigma_{n_2}+2\sigma_{nf}+\phi_2(\sigma_{nf}-\sigma_{n_2})}\right], \tag{9}$$

where $K_{nf}=\frac{K_{n_1}+2K_f-2\phi_1(K_f-K_{n_1})}{K_{n_1}+2K_f+\phi_1(K_f-K_{n_1})}\times K_f$, $\sigma_{nf}=1+\frac{3\left(\frac{\sigma_{n_1}}{\sigma_f}-1\right)\phi_1}{2+\frac{\sigma_{n_1}}{\sigma_f}-\left(\frac{\sigma_{n_1}}{\sigma_f}-1\right)\phi_1}$.

The base fluid Ethylene glycol ($C_2H_6O_2$) and nanoparticle's thermophysical properties are mentioned in Table 1 [23].

Here μ_f presents the dynamic viscosity of $C_2H_6O_2$. K_f, K_{n_1} and K_{n_2} denote the thermal conductivity of base fluid, graphene and copper respectively. ϕ_1 and ϕ_2 indicate the volume fraction of graphene nanoparticle and copper nanoparticle respectively. σ_f, σ_{n_1} and σ_{n_2} is the notation of electrical conductivity of $C_2H_6O_2$, Graphene and Copper. ρ_f, ρ_{n_1} and ρ_{n_2} is the notation of density of $C_2H_6O_2$, Graphene and Copper. $(\rho c_p)_f$, $(\rho c_p)_{n_1}$ and $(\rho c_p)_{n_2}$ is the notation of heat capacity of $C_2H_6O_2$, Graphene and Copper. Boundary conditions are taken as:

$$u=0, v=\frac{dh}{dt}, T=T_H \ at\ y=h(t) \tag{10}$$

$$\frac{\partial u}{\partial y}=0, v=0, \frac{\partial T}{\partial y}=0\ at\ y=0 \tag{11}$$

Similarity transformations are given as [27]

$$\eta=\frac{y}{H\sqrt{1-\alpha t}}, u=\frac{\alpha x}{2(1-\alpha t)}f'(\eta), v=\frac{-\alpha H}{2\sqrt{(1-\alpha t)}}f(\eta), \theta=\frac{T}{T_H} \tag{12}$$

Using the similarity transformations given in equation (12) into the PDEs (2) to (4) and eliminating the pressure terms by cross- differentiations of equations (2) and (3), the resultant ordinary differential equation is mentioned from equation (13) to (14) as follows:

$$S\left(\frac{A_1}{A_4}\right)\left[3f''+\eta f'''+f'f''-ff'''\right]+M^2\left(\frac{A_5}{A_4}\right)f''=f^{iv} \tag{13}$$

$$\theta''+S.Pr\left(\frac{A_2}{A_3}\right)[f\theta'-\eta\theta']+M^2\left(\frac{A_5}{A_3}\right)Pr.E\,cf'^2-G.\theta=0 \tag{14}$$

$$\eta=0\Rightarrow f''(0)=0, f(0)=0, \theta'(0)=0 \tag{15}$$

$$\eta=1\Rightarrow f'(1)=0, f(1)=1, \theta(1)=1 \tag{16}$$

Where $S=\frac{\alpha H^2}{2\nu_f}$, $A_1=\frac{\rho_{hnf}}{\rho_f}$, $A_2=\frac{(\rho C_p)_{hnf}}{(\rho C_p)_f}$, $A_3=\frac{K_{hnf}}{K_f}$, $A_4=\frac{\mu_{hnf}}{\mu_f}$, $A_5=\frac{\sigma_{hnf}}{\sigma_f}$. $Pr=\frac{\mu_f(\rho C_p)_f}{\rho_f K_f}$ is the Prandtl number, $E_C=\frac{\rho_f}{(\rho C_p)_f T_H}\left(\frac{\alpha x}{2(1-\alpha t)}\right)^2$ noting the Eckert number, $M=HB_0\sqrt{\frac{\sigma_f}{\mu_f}}$ is the magnetic number, $G=\frac{Q_0 H^2}{K_{nf}}$ denotes the

Table 1. Thermophysical properties of Ethylene glycol and nanoparticles [23]

Thermo-physical properties	$\rho(kg/m^3)$	$c_p(J/kgK)$	$K(W/mK)$	$\sigma(S/m)$
Graphene	2250	2100	2500	1×10^{-7}
Copper	8993	385	401	5.96×10^{7}
Ethylene glycol	1114	2415	0.252	5.5×10^{-6}

Table 2. Verification of $-\theta'(1)$ when S = 0.5, G = 0 and M = 0

Pr	Ec	$-\theta'(1)$ Mustafa et al.[39]	$-\theta'(1)$ Acarya et al. [40]	$-\theta'(1)$ Present work
0.5	1.0	1.5222	1.5222	1.5224
1.0	1.0	3.0263	3.0263	3.0265
2.0	1.0	5.9805	5.9805	5.9803
5.0	1.0	14.3439	14.4394	14.4397
1.0	0.5	1.5132	1.5131	1.5131
1.0	1.2	3.6315	3.6315	3.6318
1.0	2.0	6.0526	6.0526	6.0526
1.0	5.0	15.1316	15.1316	15.1315

coefficient of absorption. Where ϑ_f indicates the kinematic coefficient of viscosity.

The coefficient of skin-friction C_f and the Nusselt number Nu can be expressed as

$$C_f = \frac{\mu_{hnf}\left(\frac{\partial u}{\partial y}\right)_{y=h(t)}}{\frac{1}{2}\rho_{hnf}\left(\frac{dh}{dt}\right)^2} = \frac{4\mu_{hnf}}{H^2\rho_{hnf}\alpha}\frac{f''(1)}{\delta} \quad (17)$$

$$Nu = \frac{-HK_{hnf}\left(\frac{\partial T}{\partial y}\right)_{y=h(t)}}{K_f T_H} = \frac{-Nu_r}{\sqrt{(1-\alpha t)}}. \quad (18)$$

Where $Nu_r = A_3\theta'(1)$ and $\delta = \frac{H\sqrt{(1-\alpha t)}}{x}$.

NUMERICAL METHOD IMPLEMENTATION

The majority of natural processes are characterized by highly intricate nonlinear dynamics, typically described by nonlinear differential equations. Attaining a closed-form exact solution under such circumstances proves to be unattainable. In these situations, researchers seek approximate solutions through either numerical methods or analytical techniques. Numerical solutions can be obtained employing diverse methods like the finite difference method [31], finite volume method [32], finite element method (FEM) [33], reproducing kernel algorithm [34-37] and shooting method [38]. The solution of the present problem is obtained by using shooting method along with Runge-Kutta fourth order technique. In order to find the solution of transformed ordinary differential equations (13) and (14) subject to boundary conditions (15) and (16), the following steps are used:

- To solve the equations (13) and (14), first converted into a system of six first-order differential equations.
- To find the solution of the system of ordinary differential equations, the initial values of $f''(0)$ and $\theta'(0)$ are found using the shooting method along with Runge-Kutta fourth order technique.
- After the grid Independence analysis, the step size selected is 0.001 throughout the computation.
- A tolerance error of 10^{-6} is chosen. The entire process is repeated until the desired accurate result is obtained.

Characteristics of Shooting Technique

- Shooting method converts boundary value problem to initial value problem. Then initial value problem needs to be solved and initial guesses are to be found in each iteration. This process will continue until solution satisfies the given boundary conditions.
- The convergence of shooting method depends on initial guess. Poor initial guess may decrease the rate of convergence or possibly solution may diverge.

Characteristics of Runge-Kutta Fourth Order Method

- Runge-Kutta fourth order method is used to solve initial value problem with high accuracy.
- In Runge-Kutta fourth order method, step size can be adjusted during the solving process.

Validation of Present Finding

In order to validate the numerical solution obtained using the method described in above section, a comparison of the Nusselt number at the upper plate is performed with the earlier published results and are presented Table [2].

It is noted from Table 2 that this manuscript is in excellent agreement with the earlier published manuscripts ([39-40]).

RESULTS AND DISCUSSIONS

In this section, all the results for velocity temperature, skin friction coefficient and Nusselt number, computed using the numerical method as described in previous section are presented graphically in Figures 2 to 12. Impact of various physical parameter M = 0.5, Pr =11, Ec = 0.05, S = 0.5, G = 0.1 and different values of nano particles volume fraction on hybrid nanofluid velocity (from Figures 2 and 3) and temperature (from Figures 4 to 6) is discussed and analyzed. In all graphical representations the results are displayed for three different cases of fluid flow: (1) Base fluid (Ethylene

Glycol- $C_2H_6O_2$) only using solid lines, (2) mono-nanofluid ($C_2H_6O_2$ + Graphene) using dashed lines and (3) Hybrid nanofluid ($C_2H_6O_2$ + Graphene + Copper) using dotted lines. Throughout the manuscript ϕ_1 and ϕ_2 represents graphene and Copper nanoparticle volume fractions.

Velocity Profile

The velocity profiles of the flow problem are presented in Figures 2 and 3, against the magnetic field and squeezing number. Figure 2 illustrates the impact of magnetic field nanoparticles volume faction on hybrid nanofluid velocity. It is notice that due to an increase in the magnetic field, a very small reduction in velocity of the hybrid nanofluid up to central region while the opposite nature is observed after that. This phenomenon is happening due to Lorentz force up to central region and after that due to the continuity equation. It also shows that in case of mono-nanofluid ($\phi_1 = 0.05$ and $\phi_2 = 0$), velocity is higher than the base fluid and lower than hybrid nanofluid ($\phi_1 = 0.025$ and $\phi_2 = 0.025$) up to central region.

Figure 3 demonstrates the influence of the Squeeze number on hybrid nanofluid velocity. It is evident that the Squeeze number decreases the hybrid nanofluid velocity, but the opposite nature is visible as the distance between the channels increases. Further, increase in squeezing number does not seem to affect the velocity abnormally as we can see a very small variations in velocity against *S*. It also shows that in the case of the mono- nanofluid ($\phi_1 = 0.05$ and $\phi_2 = 0$), the velocity is higher than the base fluid and lower than the hybrid nanofluid ($\phi_1 = 0.025$ and $\phi_2 = 0.025$) up to the central region.

Temperature Profile

The temperature profile for flow problem is represented in Figures 4 to 6 against varying values of magnetic parameter, Eckert number and absorption parameter.

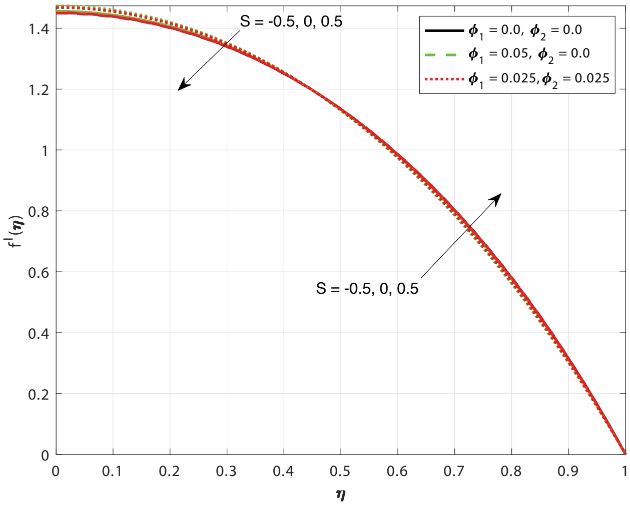

Figure 3. Varation in *S* values cause various velocity profiles.

It is clearly noted from Figure 4 that the hybrid nanofluid temperature is enhanced due to the increase in the magnetic field. This is because the fluid will face more difficulties to flow against the magnetic field.

Figure 5 shows that enhancing the Eckert number has the nature to enhance the temperature of the hybrid nanofluid. The Eckert number represents the ratio of kinetic energy to enthalpy. Some part of energy converts to kinetic energy; therefore, in the boundary layer, viscous dissipation can enhance the temperature. It is also noted that the hybrid nanofluid temperature increases when the nanoparticle volume is increased. It also shows that in the case of the mono-nanofluid ($\phi_1 = 0.05$ and $\phi_2 = 0$), the temperature is higher than the base fluid and lower than the hybrid nanofluid ($\phi_1 = 0.025$ and $\phi_2 = 0.025$). Figure 6 shows

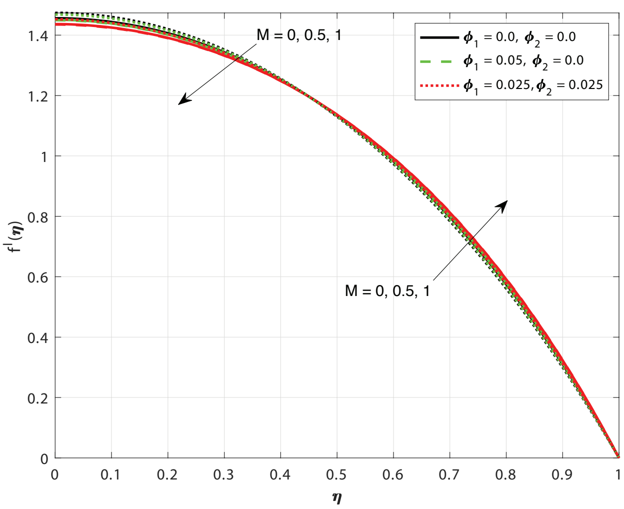

Figure 2. Varation in M values causes various velocity profile.

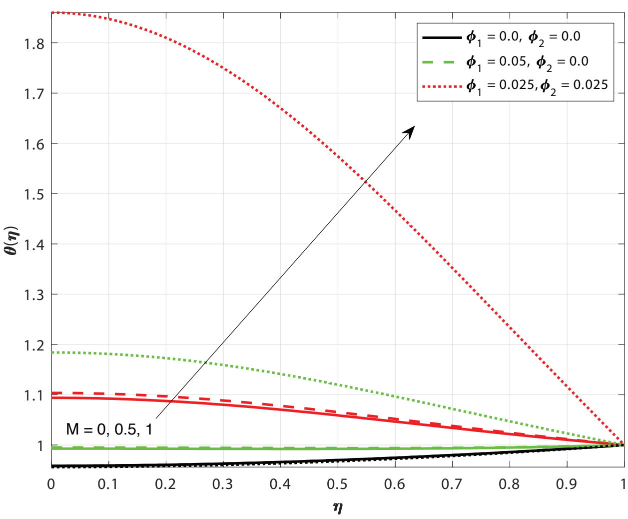

Figure 4. Varation in *M* values cause various temperature profiles.

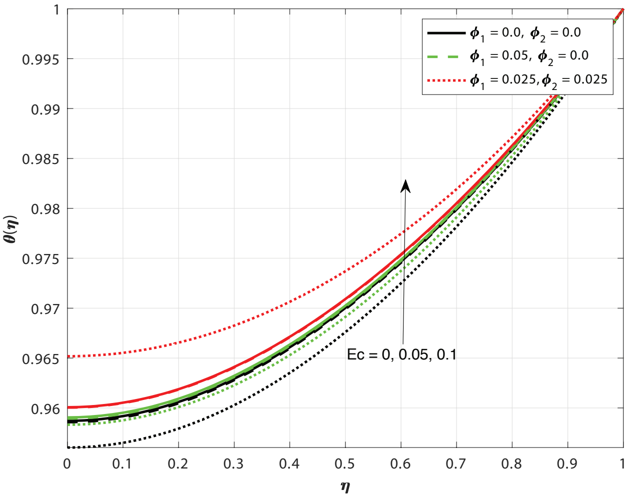

Figure 5. Varation invalues of Ec cause various temperature profiles.

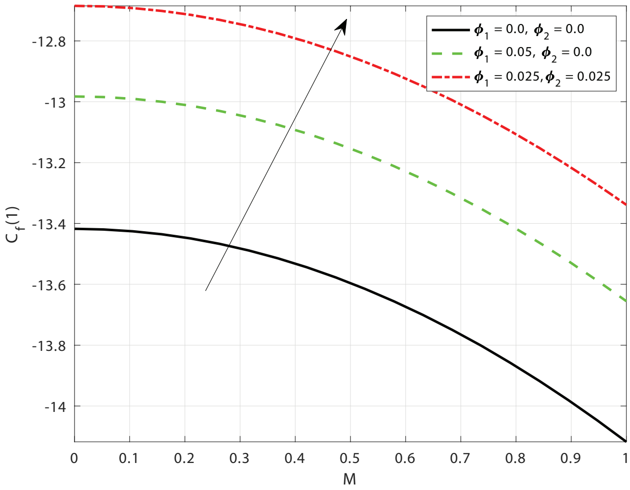

Figure 7. Varation in values of M and ϕ cause various C_f profiles.

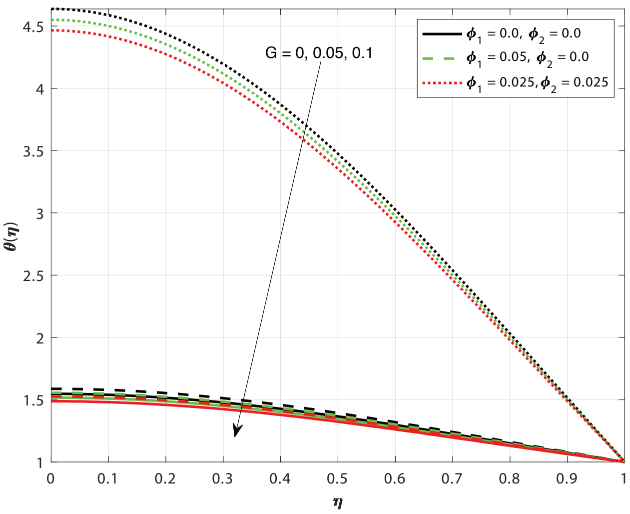

Figure 6. Varation invalues of G cause various temperature profiles.

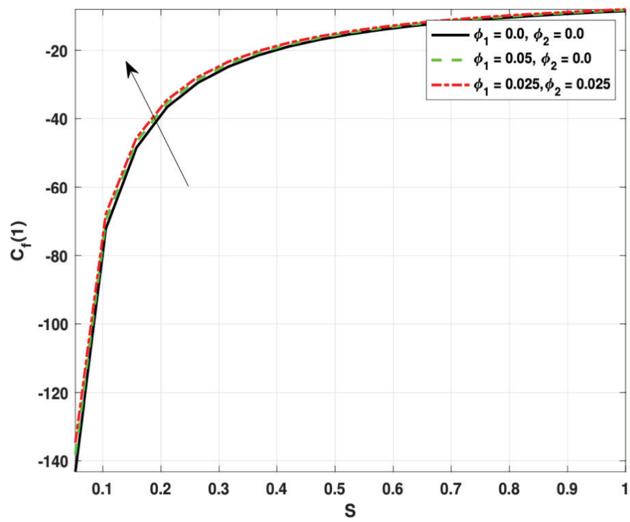

Figure 8. Varation in values of S and ϕ cause various C_f profiles.

that due to the enhancement of the absorption parameter, the temperature of the hybrid nanofluid velocity is reduced because of the increment of the absorption capacity of the fluid. It also shows from Figure 4 to 6 that in case of mono-nanofluid ($\phi_1 = 0.05$ and $\phi_2 = 0$), temperature is higher than base fluid and lower than hybrid nanofluid ($\phi_1 = 0.025$ and $\phi_2 = 0.025$).

Skin Friction and Nusselt Number Profile

The quantities of engineering interests like skin friction coefficient and Nusselt number profiles against the pertinent flow parameter is displayed in figures 7 to 12. Figures 7 and 8 presents the impact of M and S on C_f at the channel's upper plate. From Figure 7, It is visible that C_f is reducing at upper plate due to enhancement of M and opposite behavior of C_f is observed due to increase in S. It is also noted that in case of mono-nanofluid ($\phi_1 = 0.05$ and $\phi_2 = 0$), C_f is higher than base fluid and lower than hybrid nanofluid ($\phi_1 = 0.025$ and $\phi_2 = 0.025$).

Figures 9 to 12 presents the impact of M, G, S and Ec on Nu at the upper plate of the channel. From Figure 9 it is noted that when magnetic parameter is increased from 0 to 2, a 10.01% of relative increment in heat transfer rate is reported. Figure 10 which displays that the Nusselt number is a decreasing function of absorption parameter G, to be exact, we reported a relative decline of 115.24% in Nusselt number when G is varied from 0 to 1. It is observed that there is a 34.748% of decrease in Nusselt number as the value of S increases from 0 to 1, whereas an increase of 18.28% of heat transfer rate is noted for hybrid nanofluid as compared

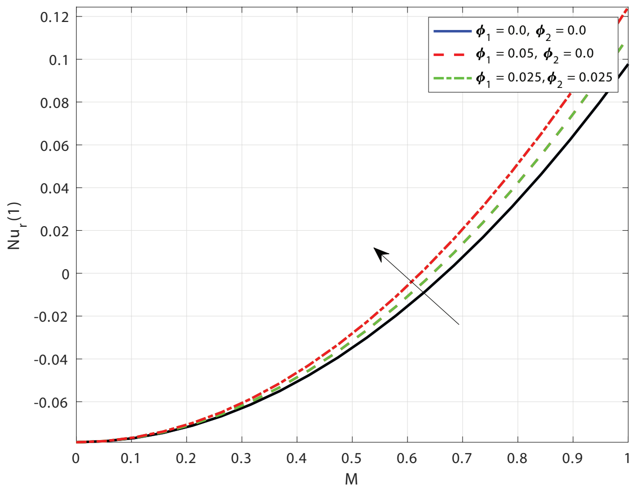

Figure 9. Varation in values of M and ϕ cause various N_u profiles.

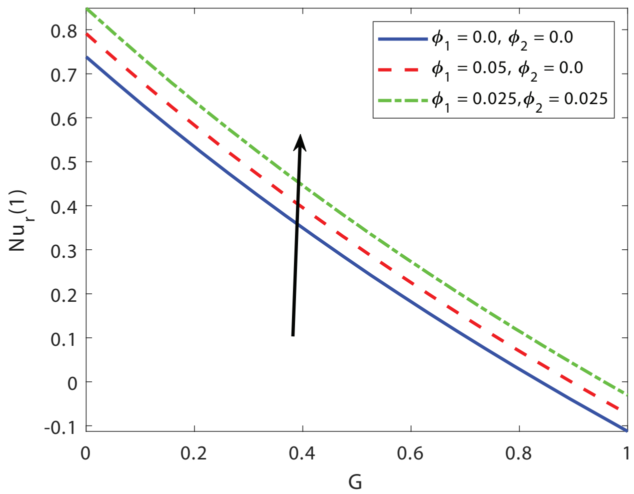

Figure 10. Varation in values of G and ϕ cause various N_u profiles.

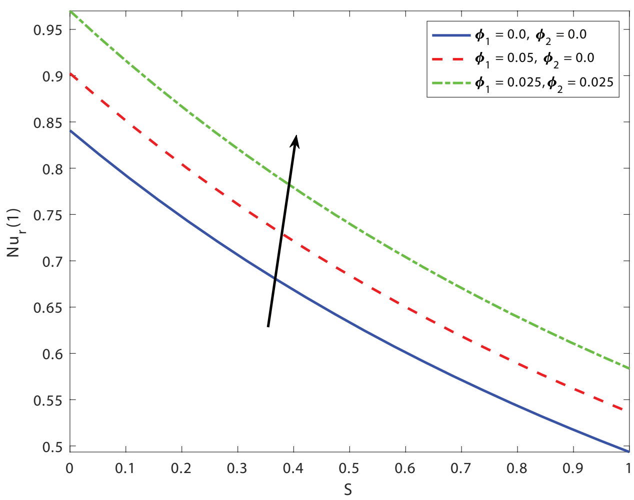

Figure 11. Varation in values of S and ϕ cause various N_u profiles.

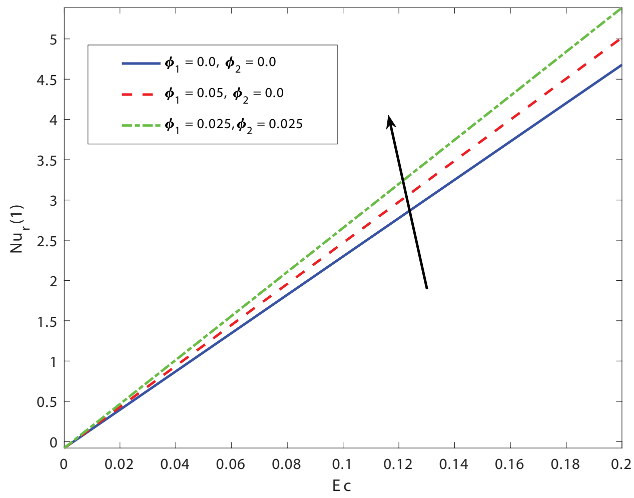

Figure 12. Varation in values of Ec and ϕ cause various N_u profiles.

to base fluid. Similarly in Figure 12 the Eckert number Ec demonstrated an increasing nature of Nusselt number against it. The investigation revealed a huge relative increase of 31.2% in Nusselt number when Ec is varied from 0 to 0.1. It is also noted that in the case of the mono-nanofluid ($\phi_1 = 0.05$ and $\phi_2 = 0$), Nu is higher than the base fluid and lower than the hybrid nanofluid ($\phi_1 = 0.025$ and $\phi_2 = 0.025$). Another aspect worth mentioning is that the rate of heat transfer in base fluid, mono-nanofluid and hybrid nanofluid is almost equal for smaller values of magnetic parameter M and Eckert number Ec, however with increasing value of M and Ec the effect of different type of fluid on Nusselt number becomes prominent. This shows that the magnetic field and Eckert number both influences the effect of nanoparticles on heat transfer rate.

CONCLUSION

This article presents the comparative study of flow and heat transfer characteristics of three different type of fluids namely (1) Base fluid (Ethylene Glycol- $C_2H_6O_2$) (2) Mono-nanofluid ($C_2H_6O_2$ + Graphene) and (3) hybrid nanofluid ($C_2H_6O_2$ + Graphene + Copper) passing through a squeezing channel. The study also takes into account the combined effects of transverse magnetic field, heat absorption and Joule dissipation. The behavior of fluid velocity, temperature, skin friction coefficient and Nusselt number are analyzed. The major findings of the present investigation are listed below:

- The hybrid nanofluid velocity is going down due to increase in magnetic field till central region and after that opposite tendency is visible.
- The nature of temperature is to grow up by enhancing due to magnetic field, Joule dissipation while opposite behavior due to enhancing of absorption parameter.

- Local skin friction at upper plate is enhancing due to enhancement of S and opposite behavior happened due to enhancement in M.
- The local Nusselt number at the upper plate is enhancing due to enhancement of M and Ec and opposite behavior happened due to enhancement in G and S.

The heat transfer rate as well as skin friction coefficient, for hybrid nanofluid found to be higher than that of both mono-nanofluid and base fluid.

NOMENCLATURE

Symbol

u	Velocities of hybrid nanofluid in the x- direction
v	Velocities of hybrid nanofluid in the y- direction
T	Temperature of hybrid nanofluid
p	Pressure in hybrid nanofluid
ρ_{hnf}	Density of hybrid nanofluid
ρ_f	Density of $C_2H_6O_2$ (base fluid)
ρ_{n_1}	Density of graphene
ρ_{n_2}	Density of copper
ϑ_{hnf}	Kinematic viscosity of hybrid nanofluid
K_{hnf}	Thermal conductivity of hybrid nanofluid
K_f	Thermal conductivity of the base fluid
K_{n_1}	Thermal conductivity of graphene
K_{n_2}	Thermal conductivity of copper
Q	Heat absorption coefficient of hybrid nanofluid
σ_{hnf}	Electrical conductivity of the hybrid nanofluid
σ_f	Electrical conductivity of base fluid
σ_{n_1}	Electrical conductivity of graphene nanoparticle
σ_{n_2}	Electrical conductivity of copper nanoparticle
$B(t)$	The strength of applied magnetic field
μ_f	Dynamic viscosity of base fluid
ϕ_1	Volume fraction of graphene nanoparticle

ACKNOWLEDGEMENTS

One of the author is grateful to the VIT-AP University for providing all necessary support to carry out this research.

AUTHORSHIP CONTRIBUTIONS

Authors equally contributed to this work.

DATA AVAILABILITY STATEMENT

The authors confirm that the data that supports the findings of this study are available within the article. Raw data that support the finding of this study are available from the corresponding author, upon reasonable request.

CONFLICT OF INTEREST

The author declared no potential conflicts of interest with respect to the research, authorship, and/or publication of this article.

ETHICS

There are no ethical issues with the publication of this manuscript.

REFERENCES

[1] Choi SUS, Eastman JA. Enhancing thermal conductivity of fluids with nanoparticles. Development and applications of non-Newtonian flows. Argonne National Lab (ANL), Argonne, IL (United States); 1995.
[2] Buongiorno J. Convective transport in nanofluids. ASME J Heat Transf 2006;128:240–250. [CrossRef]
[3] Izadi M, Ghalambaz M, Mehryan SAM. Location impact of a pair of magnetic sources on melting of a magneto-ferro phase change substance. Chin J Phys 2020;65:377–388. [CrossRef]
[4] Hajjar A, Mehryan SAM, Ghalambaz M. Time periodic natural convection heat transfer in a nano-encapsulated phase-change suspension. Int J Mech Sci 2020;166:105243. [CrossRef]
[5] Alsabery AI, Hashim I, Hajjar A, Ghalambaz M, Nadeem S, Pour MS. Entropy generation and natural convection flow of hybrid nanofluids in a partially divided wavy cavity including solid blocks. Energies 2020;13:2942. [CrossRef]
[6] Mishra MK, Seth GS, Sharma R. Scrutiny of heat transfer and nanoparticle migration within a channel filled with nanofluid. Heat Transf 2020;49:2770–2788. [CrossRef]
[7] Mishra MK, Seth GS, Sharma R. Navier's slip effect on mixed convection flow of non-Newtonian nanofluid: Buongiorno's model with passive control approach. Int J Comput Appl Math 2019;5:1–23. [CrossRef]
[8] Castro Neto AH, Guinea F, Peres NMR, Novoselov KS, Geim AK. The electronic properties of graphene. Rev Mod Phys 2009;81:109–162. [CrossRef]
[9] Chung C, Kim YK, Shin D, Ryoo SR, Hong BH, Min DH. Biomedical applications of graphene and graphene oxide. Acc Chem Res 2013;46:2211–2224. [CrossRef]
[10] Upadhya SM, Raju CSK. Unsteady flow of Carreau fluid in a suspension of dust and graphene nanoparticles with Cattaneo-Christov heat flux. J Heat Transf 2018;140:092401. [CrossRef]
[11] Bhattacharyya A, Sharma R, Mishra MK, Chamkha AJ, Mamatha E. Numerical and statistical analysis of dissipative and heat absorbing graphene Maxwell nanofluid flow over a stretching sheet. J Nanofluids 2021;10:600–607. [CrossRef]
[12] Devi SPA, Devi SSU. Numerical investigation of hydromagnetic hybrid Cu-Al2O3/water nanofluid flow over a permeable stretching sheet with suction. Int J Nonlinear Sci Numer Simul 2016;17:249–257. [CrossRef]

[13] Suresh S, Venkitaraj K, Selvakumar P, Chandrasekar M. Synthesis of Al2O3-Cu/water hybrid nanofluids using two-step method and its thermophysical properties. Colloids Surf A 2011;388:41−48. [CrossRef]

[14] Devi SSU, Devi SPA. Numerical investigation of three-dimensional hybrid Cu-Al2O3/water nanofluid flow over a stretching sheet with effecting Lorentz force subject to Newtonian heating. Can J Phys 2016;94:490−496. [CrossRef]

[15] Prakash M, Devi S. Hydromagnetic hybrid Al2O3-Cu/water nanofluid flow over a slendering stretching sheet with prescribed surface temperature. Asian J Res Soc Sci Humanit 2016;6:1921−1936. [CrossRef]

[16] Bahiraei M, Mazaheri N. Application of a novel hybrid nanofluid containing graphene-platinum nanoparticles in a chaotic twisted geometry for utilization in miniature devices: thermal and energy efficiency considerations. Int J Mech Sci 2018;138:337−349. [CrossRef]

[17] Aziz A, Jamshed W, Ali Y, Shams M. Heat transfer and entropy analysis of Maxwell hybrid nanofluid including effects of inclined magnetic field. Joule heating and thermal radiation. Discrete Contin Dyn Syst Ser A 2020;13:2667−2690. [CrossRef]

[18] Yashkun U, Zaimi K, Ishak A, Pop I, Sidaoui R. Hybrid nanofluid flow through an exponentially stretching/shrinking sheet with mixed convection and Joule heating. Int J Numer Methods Heat Fluid Flow 2020;31:1930−1950. [CrossRef]

[19] Rafique K, Mahmood Z, Khan U. Mathematical analysis of MHD hybrid nanofluid flow with variable viscosity and slip conditions over a stretching surface. Mater Today Commun 2023;36:106692. [CrossRef]

[20] Rashid I, Zubair T, Asjad MI, Irshad S, Eldin SM. The MHD graphene-CMC-water nanofluid past a stretchable wall with Joule heating and velocity slip impact: coolant application. Front Phys 2023;10:1065982. [CrossRef]

[21] Anjali SP, Ganga B. Effects of viscous and Joule's dissipation on MHD flow, heat and mass transfer past a stretching porous surface embedded in a porous medium. Nonlinear Anal Mod Control 2009;14:303−314. [CrossRef]

[22] Daniel YS, Aziz ZA, Ismail Z, Salah F. Effects of thermal radiation, viscous and Joule heating on electrical MHD nanofluid with double stratification. Chin J Phys 2017;55:630−651. [CrossRef]

[23] Sharma R, Hussain SM, Raju CSK, Seth GS, Chamkha AJ. Study of graphene Maxwell nanofluid flow past a linearly stretched sheet: a numerical and statistical approach. Chin J Phys 2020;68:671−683. [CrossRef]

[24] Das S, Jana R, Chamkha AJ. Entropy generation due to unsteady hydromagnetic Couette flow and heat transfer with asymmetric convective cooling in a rotating system. J Math Model 2016;3:111−128.

[25] Seth GS, Mandal PK, Sharma R. Hydromagnetic Couette flow of class-II and heat transfer through a porous medium in a rotating system with Hall effects. J Math Model 2015;3:49−75.

[26] Noor AM, Shafie S. Magnetohydrodynamics squeeze flow of sodium alginate-based Jeffrey hybrid nanofluid with heat sink or source. Case Stud Therm Eng 2023;49:103303. [CrossRef]

[27] Shit GC, Mukherjee S. Differential transform method for unsteady magnetohydrodynamic nanofluid flow in the presence of thermal radiation. J Nanofluids 2019;8:998−1009. [CrossRef]

[28] Ullah H, Raja K, Shoaib MAZ, Nisar M, Islam KS, Weera SW, Al-Harbi N. Numerical treatment of squeezed MHD Jeffrey fluid flow with Cattaneo-Christov heat flux in a rotating frame using Levenberg-Marquardt method. Alex Eng J. 2023;66:1031−1050. [CrossRef]

[29] Kumar BP, Suneetha S. Thermal radiation and chemical reaction effects of unsteady magnetohydrodynamic dissipative squeezing flow of Casson nanofluid over horizontal channel. J Nanofluids. 2023;12:1039−1048. [CrossRef]

[30] Li S, Raghunath K, Alfaleh A, Ali F, Zaib A, Khan MI, ElDin SM, Puneeth V. Effects of activation energy and chemical reaction on unsteady MHD dissipative Darcy-Forchheimer squeezed flow of Casson fluid over horizontal channel. Sci Rep. 2023;13:2666. [CrossRef]

[31] Özişik MN, Orlande HR, Colaço MJ, Cotta RM. Finite difference methods in heat transfer. Boca Raton: CRC Press; 2017. [CrossRef]

[32] Moukalled F, Mangani L, Darwish M. The finite volume method. Springer International Publishing; 2016. [CrossRef]

[33] Reddy JN. An introduction to the finite element method. Vol. 3. New York: McGraw-Hill; 2013.

[34] Arqub OA. Numerical solutions for the Robin time-fractional partial differential equations of heat and fluid flows based on the reproducing kernel algorithm. Int J Numer Methods Heat Fluid Flow 2018;28:828−856. [CrossRef]

[35] Arqub OA. Numerical simulation of time-fractional partial differential equations arising in fluid flows via reproducing kernel method. Int J Numer Methods Heat Fluid Flow 2020;30:4711−4733. [CrossRef]

[36] Arqub OA, Smadi MA. Numerical solutions of Riesz fractional diffusion and advection-dispersion equations in porous media using iterative reproducing kernel algorithm. J Porous Media 2020;23:783−804. [CrossRef]

[37] Arqub OA, Shawagfeh N. Application of reproducing kernel algorithm for solving Dirichlet time-fractional diffusion-Gordon types equations in porous media. J Porous Media 2019;22:411−434. [CrossRef]

[38] Zaimi WMKAD, Bidin B, Bakar NA, Hamid RA. Applications of Runge-Kutta-Fehlberg method and shooting technique for solving classical Blasius equation. World Appl Sci J 2012;17:10–15.

[39] Mustafa M, Hayat T, Obaidat S. On heat and mass transfer in the unsteady squeezing flow between parallel plates. Meccanica 2012;47:1581–1589. [CrossRef]

[40] Acharya N, Das K, Kundu PK. The squeezing flow of Cu-water and Cu-kerosene nanofluids between two parallel plates. Alex Eng J 2016;55:1177–1186. [CrossRef]